Self-consistent band theory of the Fermi-surface, optical, and photoemission properties of copper*

J. F. Janak, A. R. Williams, and V. L. Moruzzi
IBM Thomas J. Watson Research Center, Yorktown Heights, New York 10598
(Received 19 September 1974)

A two-parameter self-consistent theory of the electronic structure of copper is presented. The first parameter, the exchange coefficient α appearing in Slater's $X\alpha$ theory, is adjusted so that the ground-state energy bands generate the measured Fermi surface. The second parameter, the electron-electron contribution to the effective electron mass m^* appearing in the Sham-Kohn local-density theory of excitations, is adjusted to optical-absorption data. The theory treats all electrons identically and provides a more accurate unified interpretation of Fermi-surface, optical-absorption, and photoemission data than previously obtained. We show that the transition probabilities (momentum matrix elements), while their inclusion is necessary for a convincing description of $\epsilon_2(\omega)$, can for the most part be assumed constant in the calculation of photoemission spectra. Comparison with the Chodorow potential shows that it gives excellent results for the d bands, but leads to excited-state energies which are approximately 7% too low. A detailed description is given of our computational procedures, including the generation of momentum matrix elements, $\vec{k}\cdot\vec{p}$ extrapolation, $\vec{k}$-space integration procedures and convergence tests, as well as our procedure for constructing photoemission energy distributions.

I. INTRODUCTION

Crystalline copper has for many years provided a testing ground for our theoretical understanding of the electronic structure of the nonsimple elements, i.e., metals involving d bands. Some of the reasons for this are as follows: (i) Optical data show clear structure which is unobscured by collective excitations (plasmons); (ii) Fermi-surface data of very high precision are available; (iii) it is light and therefore relatively uncomplicated by relativistic effects; (iv) it is nonmagnetic; and (v) its face-centered-cubic crystal structure is tightly packed, which makes the theoretically convenient muffin-tin approximation justifiable. The fact that copper is the only element possessing these virtues is the basis of the long-standing and continuing interest in its electronic structure.

The purpose of this paper is to describe the extent to which the optical and Fermi-surface measurements can be quantitatively explained by contemporary models for the interacting electron-ion system responsible for the macroscopic behavior. The relationship between macroscopic measurements and microscopic models is a computational chain consisting of many internally complex links, the most prominent and well studied of which are (i) the reduction of the many-electron problem to an effective one-electron problem, (ii) determination of the one-electron states, (iii) evaluation of transition probabilities between the one-electron states, (iv) interpolation between the inevitably sparse sampling of the $\sim 10^{23}$ individual one-electron states, and (v) averaging over the many states or pairs of states contributing to a given measurement. The principal uncertainty in this chain is step (i) and the information we seek is the relationship between approximations made at this level and experimentally measured quantities. Steps (ii)–(v) must be executed with sufficient precision to leave the desired relationship unobscured.

In Sec. II we summarize our results for the Fermi surface, dielectric constant $\epsilon_2(\omega)$, and photoemission spectra $D(E,\omega)$ for copper and compare with experimental quantities. Calculations of the optical properties of copper have been performed for the Chodorow[1] potential and for the self-consistent $X\alpha$ potential,[2] using the value of $\alpha = 0.77$ which we earlier found[3] by fitting Fermi-surface data. According to Sham and Kohn[4] (see also Hedin and Lundqvist[5]) application of the self-consistent ground-state potential to the excitation spectrum requires self-energy corrections. Near the Fermi energy, the self-energy corrections are expected to have the effect of increasing the excited-state energies $\tilde{E}_n(\vec{k})$ relative to the energies $E_n(\vec{k})$ computed from the ground-state potential by an amount proportional to $E_n(\vec{k}) - E_f$, i.e.,

$$\tilde{E}_n(\vec{k}) = E_n(\vec{k}) + \lambda[E_n(\vec{k}) - E_f] , \qquad (1)$$

where λ is related to the electron-electron contribution to the effective mass as described in Appendix A. We have found that the $X\alpha$ ($\alpha = 0.77$) potential, which fits the Fermi surface of copper, also gives good agreement with the optical properties of copper and the photoemission properties for photon energies up to 25 eV if the excited-state energies are assumed to have a self-energy correction of this type with $\lambda = 0.08$. Further details on the construction of the potential and the self-energy correction are given in Appendix A.

Detailed descriptions of the computational aspects of this work appear in Appendices B and C. Basically, our purpose has been to perform all the calculations required to go from a parametric description of exchange and correlation to experimentally accessible quantities. The calculations must be made with sufficient precision to test the adequacy of simple one-electron direct-transition theories of optical absorption and photoemission. The calculation also shows what is necessary to get agreement with experiment, both physically (e.g., how important are many-body effects, optical transition probabilities, etc. ?) and computationally (how many k points are required to make the calculations converge?).

Briefly, we calculate the energy bands, wave functions, and matrix elements using the Korringa-Kohn-Rostoker (KKR) method. KKR calculations are relatively costly, and we obtain the energy bands $E_n(\vec{k})$, gradients $\nabla_k E_n(\vec{k})$, and optical transition probabilities $|\langle n|\vec{p}|n'\rangle|^2$ on a mesh of $\vec{k}$ points sufficiently fine to permit accurate evaluation of integrals by using $\vec{k}\cdot\vec{p}$ extrapolation locally around each KKR point. The density of states, imaginary part of the dielectric constant, and photoemission energy distributions are calculated using the Gilat-Raubenheimer method with appropriate generalizations.

II. DENSITY OF STATES, FERMI SURFACE, DIELECTRIC CONSTANT $\epsilon_2(\omega)$, AND PHOTOEMISSION SPECTRA $D(E,\omega)$ FOR COPPER

We have carried out a series of extensive calculations designed to provide an internally consistent interpretation of photoemission, dielectric constant, de Haas–van Alphen (dHvA), and cyclotron-resonance data for copper in terms of the underlying electronic states; comparison with experiment yields information on the adequacy of the theoretical model. Where agreement is obtained, additional information (e.g., which states are responsible for optical activity at a given photon energy) can be inferred from the experimental data by examining the details of the calculations.

The foremost questions regarding the adequacy of the theoretical model are (i) the validity of the local density treatment of exchange and correlation, and (ii) the validity of the independent-particle approximation for each of the experiments considered here. Hohenberg, Kohn, and Sham[6,7] have shown that all ground-state properties can be found by self-consistently solving a single-particle Schrödinger equation with an effective ground-state one-electron potential. The exact functional dependence of this potential on the charge density is not known, nor is it known, in general, to what extent the results of the ground-state calculation apply to excited-state properties. For example, the ground-state potential implies a Fermi surface, but this surface may not be the same as the one measured experimentally,[8] even though a correspondence has been established by Sham and Kohn[4] for the case of slowly varying electron density.

A further problem exists for the optical experiments, since the one-electron picture ignores vertex corrections due to the Coulomb interaction between the excited electron and the hole left behind. (In other words, the optical properties are exactly given in terms of two- and three-particle Green's functions, which are replaced by products of one-particle Green's functions in the one-electron picture. This is an approximation even if the one-particle Green's function is known exactly.) Of the two optical experiments we consider, our single-particle model for photoemission is more approximate, in that it additionally ignores the effect of the nearby (usually less than ten monolayers) crystal surface on the excitation and transport processes.

A. Density of states

The computed density of states is shown in Fig. 1. *The energy scale in this figure, and all other figures in this paper, includes the self-energy correction of Eq.* (1). To conserve electrons, the magnitude of the density of states must also be scaled. Thus, if $\rho(E)$ is the density of states ob-

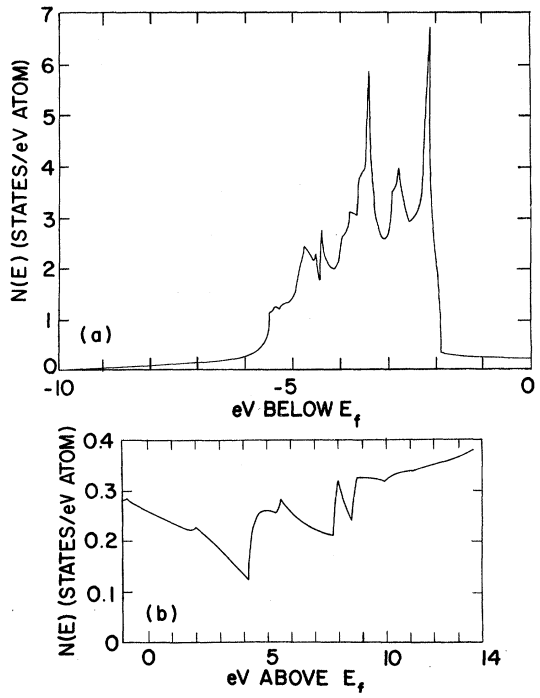

FIG. 1. Density of excitation states of copper for the $X\alpha$ ($\alpha = 0.77$) potential. The figure includes the self-energy correction of Eqs. (1) and (2).

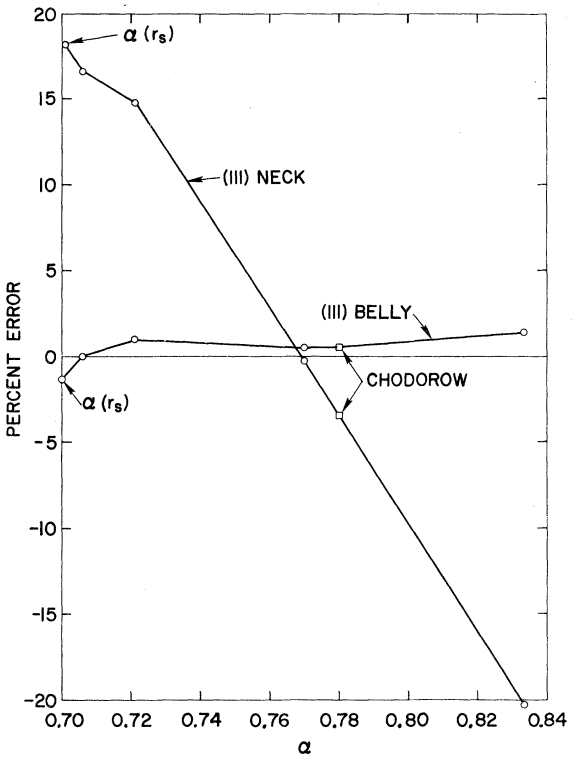

FIG. 2. Errors in de Haas–van Alphen areas, for field in [111] direction, as a function of exchange-correlation coefficient α. Points for Chodorow potential were placed so that Chodorow neck error falls on neck-error curve; points for local-density potential were placed at $\alpha = 0.7$ because the energies obtained for this potential are very close to those which would be obtained for $X\alpha$ ($\alpha = 0.7$).

tained without the self-energy correction of Eq. (1), the quantity shown in Fig. 1 is

$$N(E) = \frac{1}{1+\lambda}\,\rho\left(\frac{E}{1+\lambda}\right) . \qquad (2)$$

Studies of the d-band peaks with an energy spacing of 0.015 eV revealed no critical points; if these peaks have flat or slanted tops, they are less than 0.015 eV wide.

B. Fermi surface

Figure 2 presents the errors in some calculated Fermi-surface areas for several potentials, including the Chodorow[1] potential, and a number of self-consistent potentials: the $X\alpha$ potential of Slater[2] with $\alpha = 0.706$,[9] the local-density potential [denoted in the figure by $\alpha(r_s)$], which is an implementation of the Kohn-Sham[7] local-density theory by Hedin and Lundqvist[5] using the electron-gas results of Singwi *et al.*,[10] and the $X\alpha$ potential with $\alpha = 0.77$, the value which fits the Fermi-surface necks.[3] The belly areas vary very little with α, reflecting the constraint on the total volume of the Fermi surface. Thus, in the case of copper, one parameter (α) is being fit to one experimental datum (the neck area), and it remains to be seen whether the procedure will work equally well for materials with more complicated Fermi surfaces. It is likely, however, that the Fermi surface of any close-packed, nonrelativistic element can be fit with a self-consistent potential parametrized by α. This follows because KKR theory shows that the Fermi surface is generated by only one, two, or three material-dependent numbers, the low-l phase shifts at E_f.[11] If we regard the self-consistency process as a plausible one-parameter relationship among these few numbers, then it is likely that most details of the most complicated Fermi surface can be fit with the parameter α. Because so little information (just three phase shifts) is involved, we also expect that other parametrized forms of the exchange-correlation portion of the one-electron potential would work comparably well.

C. Dielectric constant $\epsilon_2(\omega)$

Figure 3 shows the experimental results of Johnson and Christy[12] for the interband contribution to the imaginary part of the dielectric constant, $\epsilon_2(\omega)$, and the results of our calculations for several values of λ. The value of $\lambda = 0.08$ brings the leading edge and several peak positions simultaneously into agreement with experiment.

As stated above, our calculation of $\epsilon_2(\omega)$ ignores vertex corrections due to electron-hole interactions. An earlier calculation by Mueller and Phillips[13] deviated from experiment to such an extent that these interactions were felt to be essential to a quantitative interpretation of $\epsilon_2(\omega)$. We have shown[14] that the two principal sources of the earlier deviations from experiment were inaccurate transition probabilities and inaccuracies in certain band energies implied by the Chodorow potential. Fig-

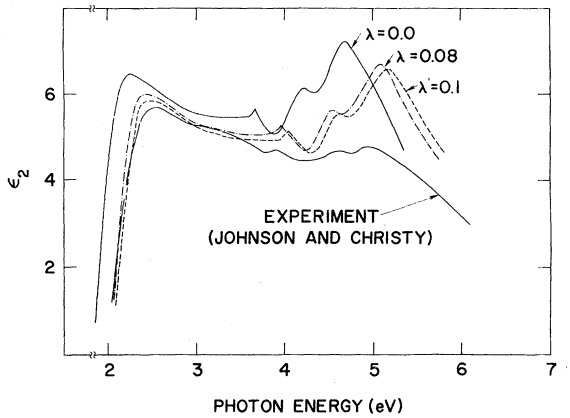

FIG. 3. Dielectric constant $\epsilon_2(\omega)$ for $\alpha = 0.77$ and several values of λ compared to experiment.

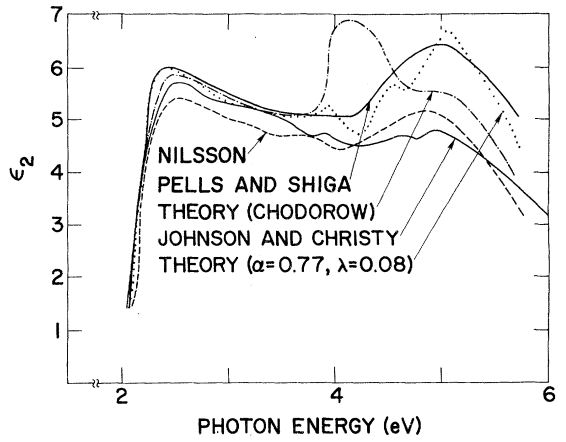

FIG. 4. Dielectric constant $\epsilon_2(\omega)$ for the two-parameter ($\alpha = 0.77$, $\lambda = 0.08$) potential and for the Chodorow potential compared to experiment. (An estimated intraband contribution has been subtracted from the Pells and Shiga data.)

ure 4 compares the $\epsilon_2(\omega)$ implied by the two-parameter potential and by the Chodorow potential with experimental measurements.[12,15,16] An encouraging aspect of Fig. 4 is that the calculated amplitude, as well as the shape, of the theoretical curve lies between the two measured curves. There is little evidence in Fig. 4 of the breakdown of the independent-particle picture.

Figure 5 shows the decomposition of the calculated $\epsilon_2(\omega)$ into contributions from different band pairs. The peak at 3.9 eV, which is seen in the theory and in the data of Johnson and Christy,[12] is due to transitions from bands 4 and 5 (which are d bands) to band 6. These transitions occur in the neighborhood of the X point of the Brillouin Zone. The peak at 4.6 eV, also seen in the data of Johnson and Christy,[12] is due to transitions from band 6 to band 7; these occur in the neighborhood of the L point. We believe the bulk of the remaining discrepancy between our two-parameter theory and the experimental data involves temperature effects in the (room temperature) Johnson-Christy[12] data and the high-ω extrapolation required for the Kramers-Kronig analysis of the Pells and Shiga[16] data. The relative amplitude of the 2- and 5-eV peaks should be more reliable in the Pells and Shiga[16] low-temperature data because ~ 30% of the 5-eV peak is due to temperature-sensitive transitions between nearly-free-electron-like bands; the amplitude of the 2-eV peak should be more reliable in the Johnson-Christy data because their technique[12] avoids normalization uncertainties introduced by Kramers-Kronig analysis.

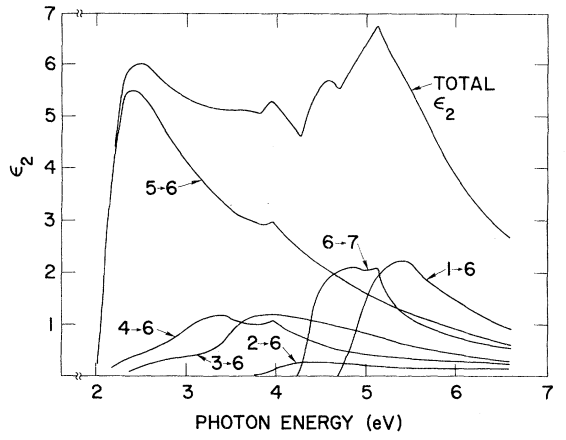

FIG. 5. Band-by-band decomposition of dielectric constant $\epsilon_2(\omega)$ for two-parameter ($\alpha = 0.77$, $\lambda = 0.08$) potential.

TABLE I. Theoretical and experimental values (eV) for energy differences in copper.

Quantity	Experiment	Theory (Chodorow)	Theory (present)
$E_F - L_3$	2.1 ± 0.1[a]	2.1	2.15
$X_{4'} - X_5$	4.0 ± 0.1[a]	3.94	3.97
$E_f - L_{2'}$	0.75[b]	0.73	0.90
$E_f - X_5$	2.0[c]	2.0	1.95
$X_5 - X_1$	3.3[d]	3.42	3.55
$L_1 - L_{2'}$	4.8[b]	4.6	5.16

[a]Reference 17.
[b]Reference 19.
[c]References 16, 18, and 19.
[d]Reference 18.

D. Characteristic features of the band structure

Information about a few level separations in the band structure can be inferred directly from the optical[16,17] and photoemission[18,19] data. Experimental values for these separations are compared with those given by our two-parameter self-consistent excitation potential in Table I. The differences between the calculated and measured quantities are not random but appear because of the following single physical effect.

As discussed in Appendix A, the λ appearing in Eq. (1) is actually the diagonal matrix element of an operator. We have neglected its n and $\vec{k}$ dependence and adjusted its value to obtain agreement with selected optical measurements. Since we are trying to fit many measurements with a single parameter, we cannot expect perfect agreement everywhere. Furthermore, the prescription for the n and $\vec{k}$ dependence of $\lambda_{n\vec{k}}$ [Eq. (A2)] shows that λ will be larger for d states than for more plane-wave-like states, and largest for the localized states at the top of the d band. Our single value of

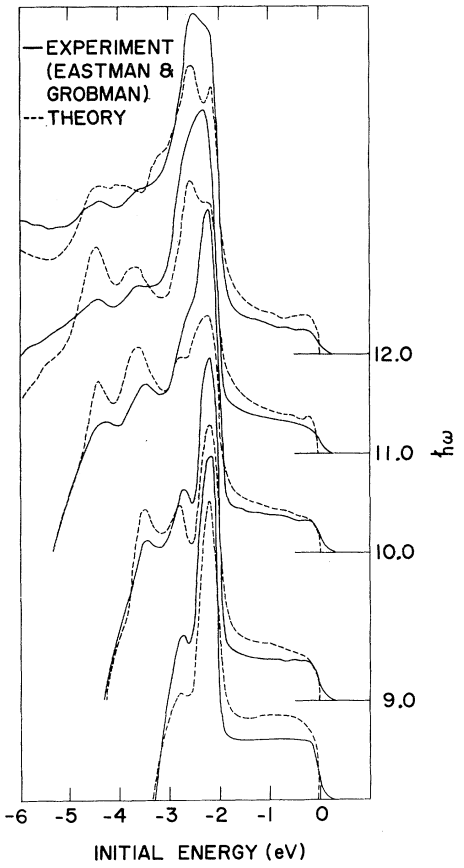

FIG. 6. Comparison of experimental and theoretical ($\alpha = 0.77$, $\lambda = 0.08$) photoemission energy distributions for $\hbar\omega$ between 8 and 12 eV.

λ is appropriate to the "average" d state; it is therefore too small for the top of the d band and too large for the plane-wave-like L_1 and $L_{2'}$ states. This is consistent with our X_5 level (top of the d bands) being too close to E_f, with the d-band width $(X_5 - X_1)$ being correct and our $L_1 - L_{2'}$ separation being too large. The experimental determination of $E_f - L_{2'}$ is less certain[19] and we believe a value of 0.85 eV is consistent with the above arguments and the fact that our ground-state potential is fit to the Fermi-surface neck radius, which in turn is directly tied to the $E_f - L_{2'}$ separation.

E. Photoemission energy distributions

Photoemission data represent the most stringent test of our simple model; there is a great deal of data to explain with no additional parameters at our disposal. Furthermore, there are several physical processes contributing to the measured quantity not present in the other measurements (surface effects on optical excitation and electron escape, electron transport, and secondary-electron production), which can complicate comparison with theory. A description of our three-step direct-transition model of the photoemission intensity $D(E, \omega)$ for a polycrystalline solid appears in Appendix C.

Figures 6–9 compare the calculated photoemission energy distributions with those measured by Eastman and Grobman[20] at a number of photon energies. The amplitude of the experimental data is arbitrary, and has been adjusted for each photon energy so that the areas under the theoretical and experimental curves are the same.

Although the relative amplitudes of certain peaks are not always as measured, the over-all curve shape as well as peak locations and their evolution with photon energy is in agreement almost everywhere. In light of the crudeness of our model, we feel there is also very little in Figs. 6–9 to warrant an appeal to more complicated physical processes, nondirect transitions, vertex corrections. etc.

F. k-space location and localization

Most of what we know concerning the $\vec{k}$-space location and localization of optical transitions in Cu

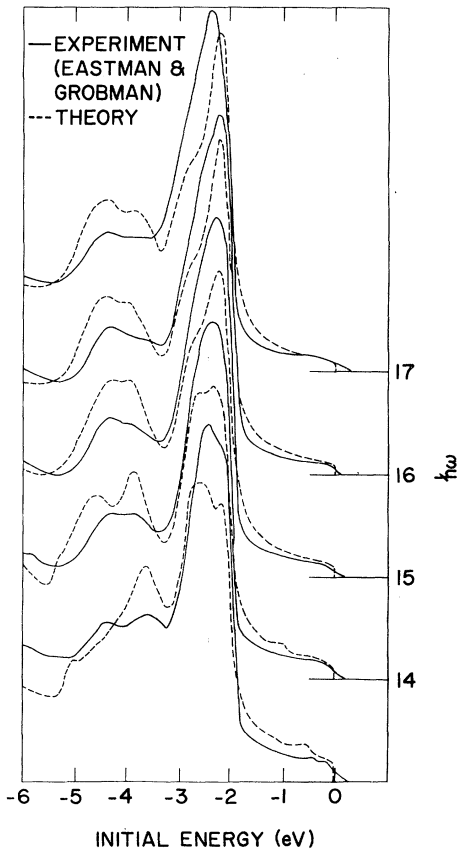

FIG. 7. Comparison of experimental and theoretical ($\alpha = 0.77$, $\lambda = 0.08$) photoemission energy distributions for $\hbar\omega$ between 13 and 17 eV.

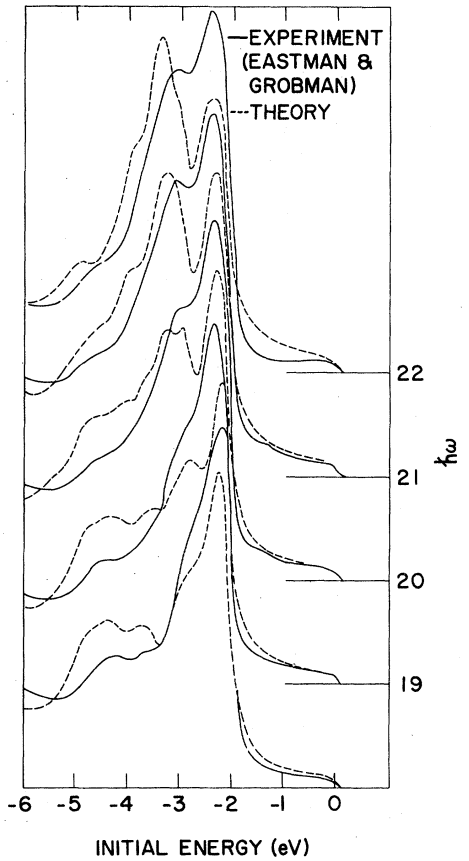

FIG. 8. Comparison of experimental and theoretical ($\alpha = 0.77$, $\lambda = 0.08$) photoemission energy distributions for $\hbar\omega$ between 18 and 22 eV.

stems from a detailed analysis of photoemission from cesiated copper reported elsewhere.[21] We have applied the same analytical techniques to higher-energy excitations, and here we summarize the results of both analyses.

Transitions between nearly-free-electron bands are almost a factor of 10 more localized in $\vec{k}$ space than are transitions out of the d bands. Transitions also tend to follow the nearly-free-electron excited-state bands. At low photon energies (5–15 eV) these bands are experiencing their first reflection from the Brillouin-zone faces and as a result optical excitations sample only the portion of the zone near the faces. In particular, since the d bands attain their full width near the zone faces this photon energy region is ideally suited to the resolution of the internal structure of the d bands. At higher photon energies (15–25 eV) the nearly-free-electron bands move back into the interior of the zone. Correspondingly, the d-band derived structure in the photoemission distribution narrows.

G. Adequacy of the Chodorow potential

A substantial fraction of all the theoretical analysis done on the electronic properties of copper has been based on the effective electron-ion interaction proposed by Chodorow in 1939.[1] Our calculations provide a basis upon which to judge the accuracy of the Chodorow potential.

Figure 2 shows that the Chodorow potential leads to Fermi-surface properties in roughly as good agreement with experiment as our two-parameter self-consistent potential.

If we compare the energy bands given by the Chodorow potential to those following from our two-parameter self-consistent potential, requiring that the Fermi levels coincide, then the d-bands of the two calculations agree to within 0.1 eV. All the other bands given by the Chodorow potential fall approximately 7% too close to the Fermi level, in agreement with our earlier investigations[14,22] and the more recent work of Wagner *et al.*[23] This provides a simple interpretation of Fig. 4: All contributions to $\epsilon_2(\omega)$ due to transitions from the d states to states near the Fermi level are accurately predicted by the Chodorow potential. The spurious peak near $\hbar\omega = 4$ eV is due to transitions

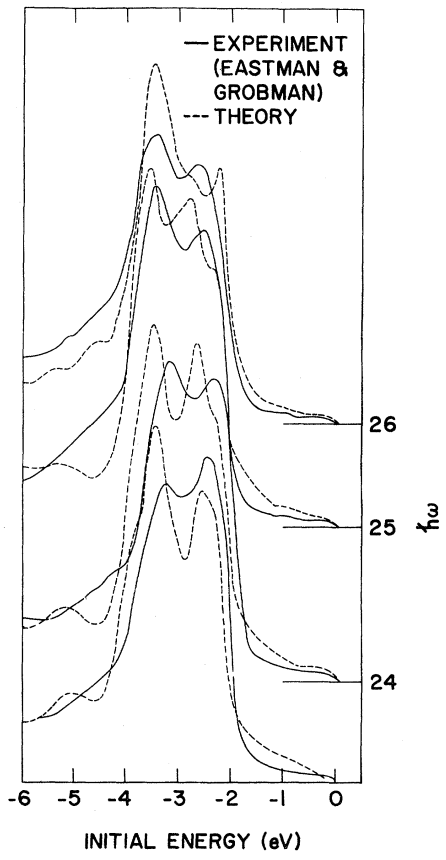

FIG. 9. Comparison of experimental and theoretical ($\alpha = 0.77$, $\lambda = 0.08$) photoemission energy distributions for $\hbar\omega$ between 23 and 26 eV.

from the Fermi level to higher levels which the Chodorow potential underestimates by 7%, as mentioned above. The accuracy of the Chodorow d bands including their distance from the Fermi level also explains the success of recent analyses[24] of photoemission data, since the latter is qualitatively dominated by the d levels and their distances from E_f.

H. Summary

We feel that our two-parameter model provides an internally consistent and remarkably accurate description of the Fermi-surface and optical measurements on copper. Both parameters of the model are physically interpretable and amenable to *a priori* calculation. The values of these parameters required to fit the data do not differ greatly from the predicted values. It is dangerous to infer a great deal from a parametrized model owing to the unknown relationship between the parameters and the effects ignored in the model. For example, our adjustment of the exchange coefficient could be compensating for our neglect of non-muffin-tin contributions to the potential and charge density. Nonetheless, the ability of our model to provide a quantitative understanding of such extensive and diverse measurements suggests to us that the fundamental conceptual building blocks out of which it is made are probably adequate; these are (i) the local-density description of the ground state, (ii) the single quasiparticle picture of optical excitation, (iii) the independent three-step (excitation, transport, and escape) picture of photoemission, and (iv) the direct ($\vec{k}$-conserving) picture of optical excitation.

ACKNOWLEDGMENTS

We are indebted to Dean Eastman and Warren Grobman for supplying the copper photoemission data, to Haskel Reich for his assistance in digitizing these data, and to Emil Cohan for system programing assistance.

APPENDIX A: PARAMETRIZED GROUND-STATE-EXCITATION POTENTIAL

In the text we have described the philosophy behind our two-parameter semiempirical potential and its ability to interpret Fermi-surface and optical data for copper; in this section we provide the theoretical justification for its particular form.

Hohenberg, Kohn, and Sham[6,7] have shown that the electronic charge density ρ implies all properties of the ground state. Furthermore, they showed[7] that ρ could be obtained by standard one-electron techniques from a Schrödinger equation containing, in addition to the usual electrostatic interaction of an electron with the nuclei and the electronic charge density, an exchange-correlation potential μ_{xc} which, while unknown in detail, is also uniquely determined by the charge density.

Most workers have assumed a local or nearly local relationship between μ_{xc} and ρ, i.e., that μ_{xc} at the spatial point $\vec{r}$ depends only on $\rho(\vec{r})$, or at most $\rho(\vec{r})$ and its low-order derivatives. We have assumed that μ_{xc} is proportional to $\rho^{1/3}$, and taken the constant of proportionality to be an adjustable parameter. If it is obtained from atomic calculations,[9] one has the $X\alpha$ method of Slater[2]; if it is allowed to vary with ρ as it would in an electron gas of slowly varying density,[7] one has the exchange-correlation potential obtained by Hedin and Lundqvist[5] from the electron-gas calculations of Singwi *et al.*[10] As stated above, we propose obtaining α, or perhaps its parametrized dependence on ρ, by fitting self-consistent one-electron calculations to Fermi-surface data (we assume that the experimental Fermi surface and the one implied by the effective one-electron potential are the same).

The second parameter in our potential deals with the excitation spectrum, and is determined independently of the ground-state parameter. If vertex corrections are neglected, the optical transition frequencies are determined by the one-electron excitation spectrum. This is obtained from the eigenvalues of the ground-state potential by including the energy dependence of the self-energy. Sham and Kohn[4] (the same results can be derived from the expressions given by Hedin and Lundqvist[5]) have shown, when the density is slowly varying, that the excited-state energies $\tilde{E}_n(\vec{k})$ are obtained from the eigenvalues $E_n(\vec{k})$ of the ground-state potential by

$$\tilde{E}_n(\vec{k}) = E_n(\vec{k}) + \lambda_{n\vec{k}}[E_n(\vec{k}) - E_f] \tag{A1}$$

for low-lying excited states near the Fermi energy, where

$$\lambda_{n\vec{k}} = \frac{\int d^3r\, |\psi_{n\vec{k}}|^2 [1 - m^*(\rho(\vec{r}))]}{\int d^3r\, |\psi_{n\vec{k}}|^2 m^*(\rho(\vec{r}))} . \tag{A2}$$

Here, m^* is the effective mass (in units of the free-electron mass) for the interacting electron gas, evaluated for each r for a density equal to the ground-state charge density $\rho(\vec{r})$, and $\psi_{n\vec{k}}(\vec{r})$ is a ground-state Bloch function.

In our parametrized potential, we take λ to be real and independent of n and $\vec{k}$, and we assume that

$$\tilde{E}_n(\vec{k}) = E_n(\vec{k}) + \lambda[E_n(\vec{k}) - E_f] ; \tag{A3}$$

we take this relationship to hold over the entire range of energies covered by dielectric-constant and photoemission experiments, and we obtain λ by fitting to experimentally observed optical-transition energies.

If $V_{xc}(\vec{r}, E)$ is the excited-state exchange-correlation potential, Eq. (A3) can be obtained by writ-

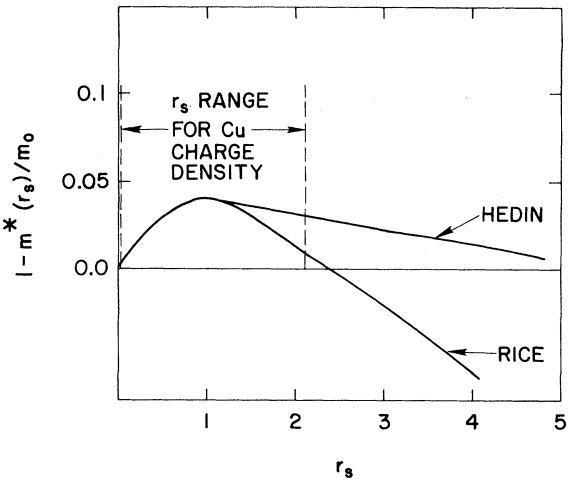

FIG. 10. $1-m^*(r_s)/m_0$ for the homogeneous electron gas as calculated by Rice (Ref. 26) and Hedin (Ref. 27). The r_s range shown includes contributions from both core and valence electrons.

ing

$$V_{xc}(\vec{r},E)=\mu_{xc}(\vec{r})+\frac{\lambda}{1+\lambda}(E-E_f)\ . \tag{A4}$$

This potential differs from the ground-state exchange-correlation potential by a term which is energy dependent but independent of position. Thus there is no change in the one-electron wave functions, and, in particular, there is no change in the momentum matrix elements evaluated using the ground-state Bloch functions. Futhermore, $\tilde{\epsilon}_2(\omega)$, the dielectric constant evaluated using the $\tilde{E}_n(\vec{k})$ defined by Eq. (A3), is related to $\epsilon_2(\omega)$ [the dielectric constant evaluated using the ground-state eigenvalues $E_n(\vec{k})$] according to

$$\tilde{\epsilon}_2(\omega)=\frac{1}{1+\lambda}\epsilon_2\left(\frac{\omega}{1+\lambda}\right), \tag{A5}$$

with a similar relation holding for the photoemission distributions. Thus, in addition to supplying a single parameter to fit the optical spectra, the assumption that λ is a constant (independent of n and $\vec{k}$) greatly simplifies the calculation by permitting the use of the ground-state momentum matrix elements.

In practice, similar values of λ are found for copper either from Eq. (A5), or by matching a single-optical-excitation energy (e.g., the d-band–Fermi-level separation) to dielectric-constant data. In this way, we have found that $\lambda=0.08$ gives a good fit to the optical properties of copper for our potential.

It is known that the effects of exchange and correlation become negligible at sufficiently high energies,[25] so we expect Eq. (A3) to fail for energies which are too far from the Fermi energy. There is little indication of this failure in the copper photoemission spectra shown in Figs. 6–9 for energies up to 25 eV above E_f. Note, however, that because the photoemission spectra are dominated by the d-bands, we do not know how sensitive they are to errors in Eq. (A3) for the higher-energy conduction bands.

We show in Fig. 10 a plot of $1-m^*(r_s)$ for the interacting electron gas as calculated by Rice[26] and Hedin.[27] Also shown is the range of r_s values covered by our ground-state copper charge density. The value of $\lambda_{n\vec{k}}$ obtained from Eq. (A2) will be some average over the shaded region of the figure. Thus, it is encouraging that photoemission is accurately described by the value of λ determined from fitting $\epsilon_2(\omega)$, and also that the value of 0.08 actually required is not much larger than that given by *ab initio* calculations.

We conclude this section by pointing out that one may view our procedure as a new level of pseudopotential theory. However, only the most uncertain portion of the self-consistent effective electron-ion interaction is empirically parametrized, whereas in ordinary pseudopotential theory, the entire electron-ion interaction is parametrized. In addition to being self-consistent, our model is not restricted to simple metals. It is our hope that during the period required to devise a practical and accurate relation between exchange-correlation potential and the charge density ρ, our scheme or similar ones can be used to interpret data and thereby guide the search for an improved theory.

APPENDIX B: COMPUTATIONAL DETAILS

Our calculations are performed in four steps: (1) iteration of the self-consistent ground-state calculation to convergence using the fast KKR method developed by the authors[28]; (2) construction of the excitation bands and momentum matrix elements on a coarse mesh in $\vec{k}$ space; (3) extrapolation from the coarse mesh to a fine mesh of $\vec{k}$ points using the $\vec{k}\cdot\vec{p}$ procedure; and (4) integration over the fine-mesh points to obtain measurable properties.

1. Excitation bands

The energy bands and wave functions are first constructed on a coarse mesh of 240 k points (13 points between Γ and X) in the irreducible $\frac{1}{48}$ of the Brillouin zone, using the KKR method. The normalization of the wave functions is obtained from the energy derivative of the KKR secular matrix, as follows. Schrödinger's equation is

$$|n\rangle=G_0V|n\rangle\ , \tag{B1}$$

where

$$G_0(\vec{r}-\vec{r}')=\frac{1}{\Omega}\sum_{\vec{K}}\frac{e^{i(\vec{k}+\vec{K})\cdot(\vec{r}-\vec{r}')}}{E-|\vec{k}+\vec{K}|^2} \tag{B2}$$

is the empty-lattice Green's function, V is the crystal potential, $|n\rangle$ is a Bloch function, and the integrations in Eq. (B1) go over one unit cell of volume Ω. This Schrödinger equation can be obtained by setting the variation of the KKR functional

$$\langle n|M|n\rangle \equiv \langle n|V - VG_0V|n\rangle \tag{B3}$$

with respect to $|n\rangle$ equal to zero. Noting that

$$\frac{\partial G_0}{\partial E} = -G_0G_0 , \tag{B4}$$

we have

$$\frac{\partial M}{\partial E} = -V\frac{\partial G_0}{\partial E}V = VG_0G_0V , \tag{B5}$$

so that

$$\langle n|\frac{\partial M}{\partial E}|n\rangle = \langle n|VG_0G_0V|n\rangle = \langle n|n\rangle = 1 \tag{B6}$$

from Eq. (B1). Thus the wave-function amplitude must be chosen so that the diagonal matrix element of $\partial M/\partial E$ is unity. Finally, noting that $M|n\rangle$ is zero if M is evaluated at the energy E_n, we have, even though the orbitals are energy dependent,

$$\langle n|\frac{\partial M}{\partial E}|n\rangle\Big|_{E=E_n} = \frac{\partial}{\partial E}\langle n|M|n\rangle\Big|_{E=E_n} = 1 . \tag{B7}$$

Because of the factors of V which appear in Eq. (B3), construction of $\langle n|M|n\rangle$ (and its energy derivative, which is obtained in practice by numerical differentiation) requires no knowledge of the wave functions outside the muffin-tin sphere.

The matrix elements of momentum are obtained from

$$\langle n|\vec{p}|n'\rangle = \frac{i\langle n|\nabla V|n'\rangle}{E_n - E_{n'}} , \tag{B8}$$

which also requires no knowledge of the wave functions outside the muffin-tin sphere, where ∇V vanishes. Diagonal matrix elements, and matrix elements between degenerate states, are obtained from the $\vec{k}$ derivative of the KKR functional M. Since

$$\frac{\partial G_0}{\partial \vec{k}} = i(\vec{r} - \vec{r}')G_0 + 2G_0\vec{p}G_0 , \tag{B9}$$

we have, if $|n\rangle$ and $|n'\rangle$ are degenerate,

$$\frac{\partial}{\partial \vec{k}}\left(\langle n|M|n'\rangle\right)_{E=E_n(k)} = \langle n|\frac{\partial M}{\partial \vec{k}}|n'\rangle = -2\langle n|VG_0\vec{p}G_0V|n'\rangle \tag{B10}$$

[the matrix element between degenerate states of $(\vec{r} - \vec{r}')VG_0V$ is zero], and thus, from Eq. (B1),

$$\langle n|\vec{p}|n'\rangle = -\frac{1}{2}\frac{\partial}{\partial \vec{k}}\langle n|M|n'\rangle . \tag{B11}$$

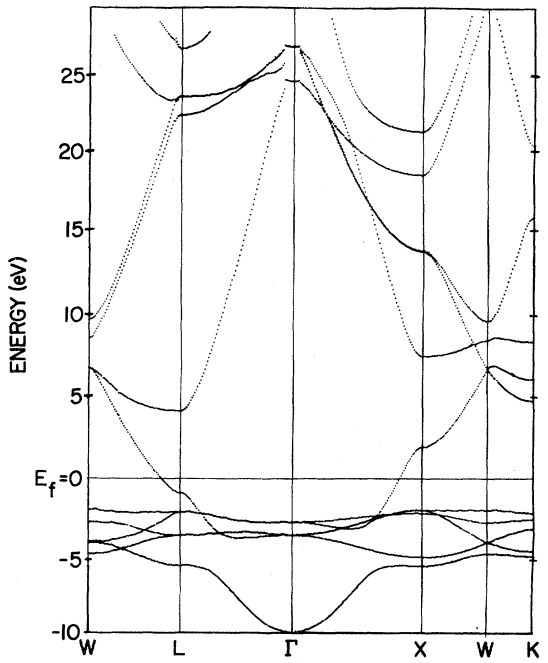

FIG. 11. Energy bands of copper for the two-parameter ($\alpha = 0.77$, $\lambda = 0.08$) self-consistent potential. Discontinuities at high energies provide a measure of errors introduced by truncation of $\vec{k}\cdot\vec{p}$ Hamiltonian.

2. $\vec{k}\cdot\vec{p}$

The third step is extrapolation from the coarse mesh to a fine mesh of points by diagonalizing a $\vec{k}\cdot\vec{p}$ Hamiltonian set up locally around each KKR point (the maximum distance over which a $\vec{k}\cdot\vec{p}$ Hamiltonian is used is thus half the maximum distance between KKR points).

The number of points required on the fine mesh is determined by the convergence of the integration procedures, and the number of coarse-mesh points needed is in turn determined by the convergence of the $\vec{k}\cdot\vec{p}$ extrapolation. The $\vec{k}\cdot\vec{p}$ convergence is also influenced to some extent by the number of energy bands included; the largest errors are expected to occur in the highest bands at each $\vec{k}$, because these will generally be the bands with the largest interactions with those states which have been omitted. Figure 11 shows the excitation bands for the self-consistent $X\alpha$ ($\alpha = 0.77$) potential (*including* the 8% self-energy spreading discussed above). Only the energies $E_n(\vec{k})$ and gradients $\nabla_k E_n(\vec{k})$ produced by the $\vec{k}\cdot\vec{p}$ procedure were used in constructing this figure, so that any inadequacies in the extrapolation would lead to discontinuities or other unphysical behavior in the plotted bands. Since the only place where this occurs is for the highest bands at Γ, it appears that $\vec{k}\cdot\vec{p}$ extrapolation is adequate for of the order of 10 bands with 240 points on the coarse mesh [so that the

maximum distance over which $\vec{k}\cdot\vec{p}$ is used is $\sim 0.07(2\pi/a)$].

3. Integration procedures

The final phase of the calculation is the integration over the fine-mesh points to obtain the density of states for the fcc structure from

$$N(E)=\frac{1}{2}\sum_n \int d^3k\,\delta(E-E_n(\vec{k})) \tag{B12}$$

(in states/Ry atom, both spins, for one atom per unit cell if E is in rydbergs and $\vec{k}$ is in units of $2\pi/a$); the dielectric constant $\epsilon_2(\omega)$, given by

$$\epsilon_2(\omega)=\frac{64\pi^2}{3\omega^2a^3}\sum_{nn'}\int d^3k\,\Theta(E_{n'}(\vec{k})-E_f)\Theta(E_f-E_n(\vec{k}))\times|\langle n|\vec{p}|n'\rangle|^2\delta(E_{n'}(\vec{k})-E_n(\vec{k})-\omega) \tag{B13}$$

(in which $\vec{k}$ is in units of $2\pi/a$; the band energies, optical matrix elements $|\langle n|\vec{p}|n'\rangle|^2$, and photon energy ω are in rydbergs; a is the lattice constant in atomic units; and $\Theta(x)$ is 1 for positive x, zero for negative x); and the photoemission energy distributions, which require the evaluation of integrals of the form

$$P_0(E,\omega)=\Theta(E-E_f)\Theta(E_f+\omega-E)\times\sum_{nn'}\int d^3k\,T(E,\vec{k})|\langle n|\vec{p}|n'\rangle|^2\times\delta(E-\omega-E_n(\vec{k}))\,\delta(E_{n'}(\vec{k})-E)\,, \tag{B14}$$

where E is the final-state energy and ω is the energy of the incident photons. This integral is the starting point of the photoemission calculations, which include in addition lifetime effects, secondary production, and escape through the crystal surface. The approximations which are used in these calculations are discussed in detail in Appendix C.

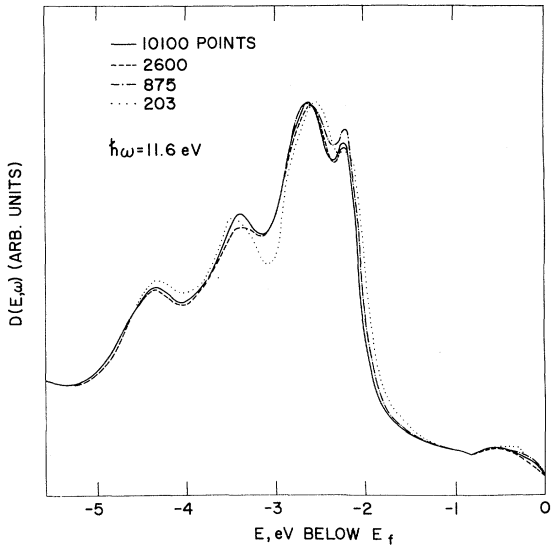

FIG. 12. Convergence of photoemission distribution $D(E,\omega)$ for $\hbar\omega=11.6$ eV for the Chodorow potential with number of $\vec{k}$ points used for integrations.

The density of states [Eq. (B12)] is computed using the Gilat-Raubenheimer (GR) method,[29] in which we consider each of the fine-mesh points to be the center of a cube, and we assume that within each cube the energy surfaces are approximately planar:

$$E_n(\vec{k})\simeq E_n(\vec{k}_0)+(\nabla_{\vec{k}}E)_{\vec{k}_0}\cdot(\vec{k}-\vec{k}_0)\,. \tag{B15}$$

The number of fine-mesh points must be large enough that this local neglect of the curvature does not lead to serious errors in the computed quantities.

The optical absorption $\epsilon_2(\omega)$ [Eq. (B13)] can be thought of as the density of states of the difference bands, and thus computed in the same way as the density of states, if it is assumed that the momentum matrix elements in each of the GR cubes are constant, equal to their values at the cube center. The number of fine-mesh points must be large enough to make this approximation reasonable, in addition to the requirement that the surfaces of constant energy difference should have small curvature in each cube.

The photoemission energy distributions [Eq. (B14)], since the integral contains two δ functions, require a somewhat different approach. As has been discussed in detail elsewhere,[30] this integral can be rewritten as a line integral along the intersection of the two surfaces defined by the δ functions, and the number of fine-mesh points must be large enough that it becomes reasonable to replace the curve of intersection of the two energy surfaces in each cube by the straight line of intersection which results when each energy surface is approximated as in Eq. (B15).

4. k convergence

Calculations of a typical photoemission energy distribution curve and of the dielectric constant $\epsilon_2(\omega)$ for various numbers of fine-mesh points in the irreducible wedge are shown in Figs. 12 and 13. Although small changes in amplitude occur as the number of fine-mesh points is increased, it is seen that a mesh of 2600 fine-mesh points is adequate for photoemission and ϵ_2 calculations; it is doubtful that the differences between the 2600-point and 10 100-point calculations are of any importance in comparing to experimental data with a resolution of 0.1 eV or more. Surprisingly, the major effect of using fewer than 2600 points is a shift in the peak positions; even the curves computed with 203 points have the correct over-all shapes, and would be adequate for comparison to experimental data of low

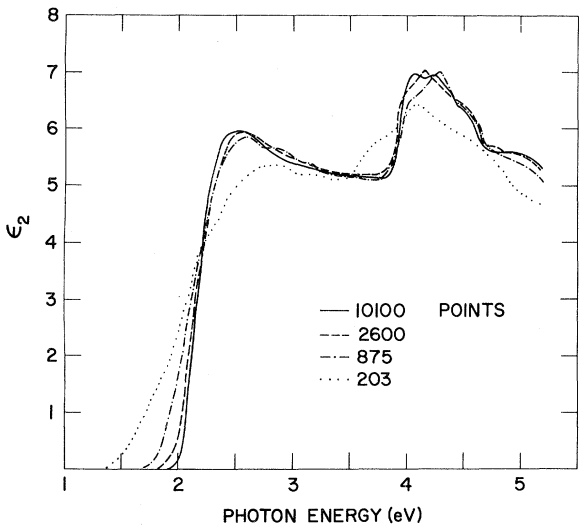

FIG. 13. Convergence of dielectric constant $\epsilon_2(\omega)$ for the Chodorow potential with number of $\vec{k}$ points used for integrations.

resolution. (An 875-point calculation over a 2-Ry energy range, including the $\vec{k}\cdot\vec{p}$ extrapolation, the density of states, dielectric constant, and one photoemission distribution, requires less than one minute of central-processing-unit time on the IBM 360/91). Although the results presented in this paper are all obtained from 10 100-point calculations, it is clear that such calculations are capable of much higher resolution than is presently attainable experimentally. This is particularly true of the photoemission calculations, where the combination of our method of obtaining bare distributions with the correct area, and the convolution with a relatively broad (~ 0.5-eV width) hole-state Lorentzian (see Appendix C) leads to quite rapid k convergence.

TABLE II. Optical matrix element $|\langle n|\vec{p}|n'\rangle|^2/2m$ in rydbergs and transition energies in rydbergs for copper (Chodorow). All nonvanishing matrix elements at Γ, L, and X are given for n and $n' \leq 7$.

Transition	Transition energy (Ry)	$\lvert\langle n\rvert\vec{p}\rvert n'\rangle\rvert^2/2m$ (Ry)
$\Gamma_{25'} \rightarrow \Gamma_1$	1.976	0.330
$L_1 \rightarrow L_{2'}$	0.344[a]	0.051
$L_3 \rightarrow L_{2'}$	0.214[a]	0.009
$L_3 \rightarrow L_{2'}$	0.214[a]	0.003
$L_3 \rightarrow L_{2'}$	0.106[a]	0.141
$L_3 \rightarrow L_{2'}$	0.106[a]	0.052
$L_{2'} \rightarrow L_1$	0.336	0.721
$X_1 \rightarrow X_{4'}$	0.540	0.042
$X_5 \rightarrow X_{4'}$	0.289	0.120
$X_{4'} \rightarrow X_1$	0.387	0.780

[a]Transitions between occupied states.

Since the band density of states is not an experimentally accessible quantity, the only justification for obtaining it to high accuracy (which may require of the order of 10^4 points) is to permit numerical integration for finding the Fermi energy. We circumvent this problem by computing the intergrated density of states, using a generalization of the GR method suitable for finding volume integrals (one can construct algebraic expressions for the volume of that portion of a cube on one side of an arbitrary plane). In this way, the Fermi energy can be obtained to an accuracy of better than 0.001 Ry from a 203-point calculation.

5. Matrix elements and band velocities

It is of some interest to determine whether it is necessary to include the momentum matrix elements in calculations of $\epsilon_2(\omega)$ and the photoemission distributions, and to see how important it is to use the electron group velocity implied by the band calculation, rather than a free-electron expression, in the transport factor appearing in the photoemission calculations [Eq. (C2)]. One expects matrix-element effects to be less important, in general, for transition and noble metals (because the d states are more localized, and the momentum matrix elements less $\vec{k}$ dependent) than they are for nearly-free-electron materials; the following discussion is pertinent only to copper, and there is some danger in trying to generalize the results to other materials.

Even if the momentum matrix elements were approximately constant over the region of $\vec{k}$ space for which a particular band pair contributes to $\epsilon_2(\omega)$ or photoemission, they can still differ for different band pairs, and thus alter the relative magnitudes of the various contributions to the total. Thus, to the extent that the contribution of a particular band pair to the optical absorption or photoemission comes from a relatively small region of $\vec{k}$ space, one would expect the main effect of omitting the momentum matrix elements to be a change in the relative peak amplitudes.

The matrix elements for some of the low bands at Γ, L, and X for the Chodorow potential for copper are given in Table II, and the effect of the matrix elements on $\epsilon_2(\omega)$ and the photoemission distributions is illustrated in Figs. 14 and 15 (both calculations were made with the Chodorow potential). It is necessary to include the matrix elements to obtain an $\epsilon_2(\omega)$ for copper which is in even qualitative agreement with experiment, but the effect of the matrix elements on the photoemission distribution is generally much less pronounced; the only place where the matrix elements have a large effect on the photoemission distributions of copper is in the neighborhood of nearly-free-electron gaps, e.g., the peak near zero initial energy

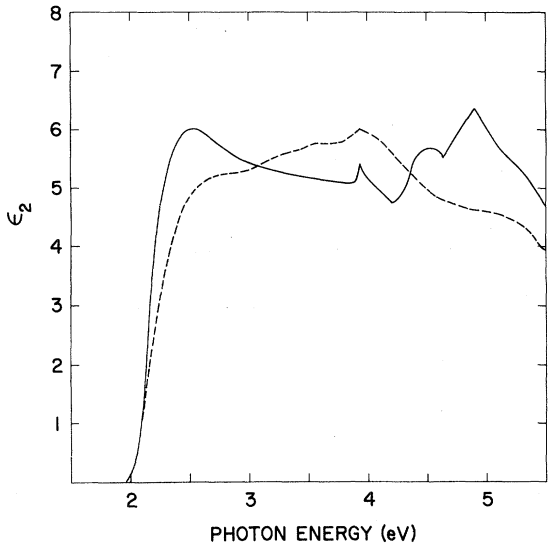

FIG. 14. Effect of momentum matrix elements on dielectric constant $\epsilon_2(\omega)$ for copper. Solid curve: including computed matrix elements; dashed curve: constant matrix elements.

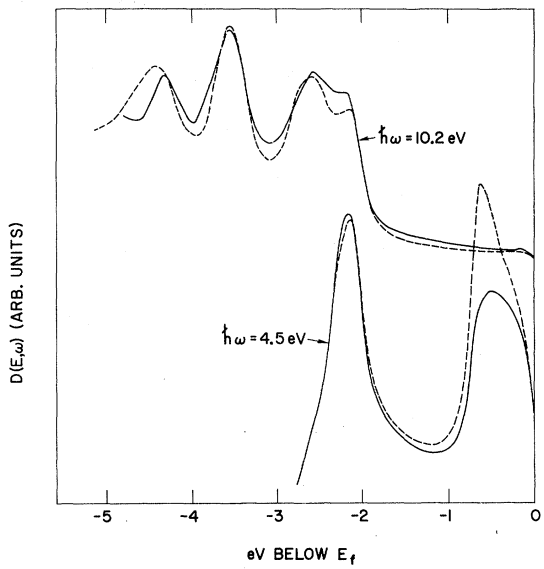

FIG. 16. Effect of band velocities on photoemission distributions for Chodorow potential for copper. Solid curves: with computed band velocities; dashed curves: with free-electron velocities.

for $\omega = 4.5$ eV in Fig. 15 (the work function in these calculations was taken to be 1.8 eV, the value appropriate to cesiated copper, in order to show effects occurring near the L gap). There are also small shifts in peak positions in the photoemission distributions; these are presumably caused by changes in peak amplitudes when there is a smoothly varying background.

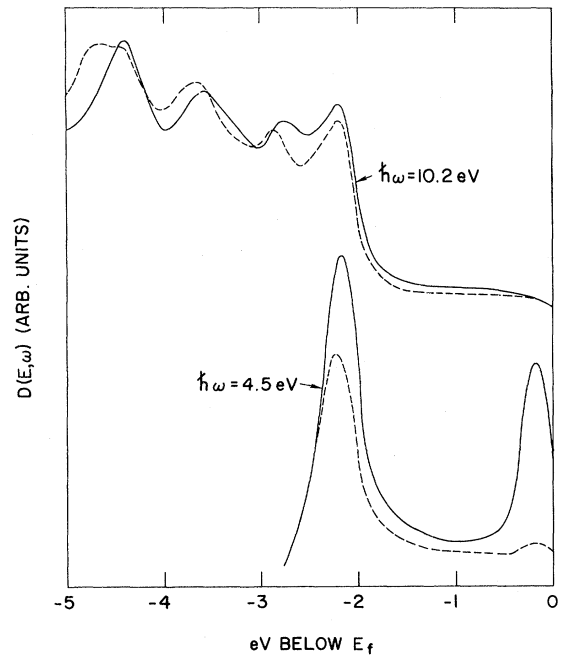

FIG. 15. Effect of momentum matrix elements on photoemission distributions for Chodorow potential for copper. Solid curve: including computed matrix elements; dashed curve: constant matrix elements.

The general conclusion is that, for copper, one can do a reasonable calculation of optical properties without matrix elements only for transitions from the d bands; unfortunately, much of the structure in $\epsilon_2(\omega)$, and that portion of photoemission data for cesiated copper which is due to transitions across the L gap, are due to transitions between sp states, and the matrix elements for these transitions must be taken into account.

Figure 16 shows photoemission distributions for the Chodorow potential for copper computed using two different electron velocities in the transport factor (see Appendix C), which is essentially the probability that an electron excited somewhere in the crystal will get to the surface without being scattered. One of the calculations in the figure was performed using the velocity obtained from the band calculation, and the other was performed assuming that the velocity of an electron with reduced wave vector $\vec{k}$ was proportional to $\vec{k}$. In general, one expects the only important differences to occur near critical points in the excited bands, where the band velocity is much smaller than the free-electron velocity (to test this, one needn't worry about including the appropriate reciprocal-lattice vector in the free-electron velocity, since it will still be much larger than the band velocity). Thus, the major differences for the copper photoemission distributions occur for transitions near the L gap (the peak near zero initial energy for

$\omega = 4.5$ eV).

It is interesting to note that omitting the band velocities in the photoemission calculations tends to compensate for omitting the matrix elements for transitions near the L gap in copper. We have not studied this effect near other nearly-free-electron transitions, either in copper or other materials, although it would constitute a useful simplification of photoemission calculations if it occurs in general.

APPENDIX C: DETAILS OF PHOTOEMISSION CALCULATIONS

In our direct-transition photoemission calculations, we assume independent excitation, transport, and escape processes (closely following Berglund and Spicer[31] in our treatment of transport and escape), and treat electron-electron scattering using Kane's[32] random-k approximation. We include both primary and secondary (once-scattered inelastically) electrons in the photoemission distribution.

The first step is to calculate the bare primary distribution according to

$$P_0(E,\omega) = \Theta(E - E_f)\Theta(E_f + \omega - E) \times \sum_{nn'} \int d^3k\, T(E,\vec{k}) |\langle n|\vec{p}|n'\rangle|^2 \times \delta(E - E_n(\vec{k}) - \omega)\,\delta(E_{n'}(\vec{k}) - E)\,, \quad \text{(C1)}$$

where $T(E,\vec{k})$ is the transport factor for excited electrons:

$$T(E,\vec{k}) = \frac{\alpha(\omega) l(E,\vec{k})}{1 + \alpha(\omega) l(E,\vec{k})}\,. \quad \text{(C2)}$$

Here $\alpha(\omega)$ is the inverse of the photon mean free path of photon energy ω, for which we use experimental values, and $l(E,\vec{k})$ is the mean free path of the excited electron,

$$l(E,k) = [\tau_e(E)/\hbar] |\nabla_{\vec{k}} E_{n'}(\vec{k})|\,. \quad \text{(C3)}$$

The relaxation time for the excited state, $\tau_e(E)$, is found from Kane's random-k approximation[32] as described below.

We calculate $P_0(E,\omega)$ by rewriting the integral as a line integral and proceeding as described in Appendix B. If neither electron nor hole states are sharp, the δ functions in Eq. (C1) should be replaced by the spectral densities of the hole and electron states:

$$\delta(E - \omega - E_n(k))\,\delta(E_{n'}(k) - E) \to A_h(E - \omega; E_n(k))\, A_e(E; E_{n'}(k))\,,$$

where we assume that

$$A_e(E; E_{n'}(k)) = \frac{\pi^{-1}\tau_e^{-1}(E)}{[E - E_{n'}(k)]^2 + [\tau_e^{-1}(E)]^2}\,, \quad \text{(C4)}$$

$$A_h(E - \omega; E_n(k)) = \frac{\pi^{-1}\tau_h^{-1}(E - \omega)}{[E - \omega - E_n(k)]^2 + [\tau_n^{-1}(E - \omega)]^2}\,, \quad \text{(C5)}$$

with $\tau_h(E)$, the relaxation time for holes, also computed from Kane's random-k approximation[32] as described below. [Equations (C4) and (C5) are identical to the usual expressions for one-electron spectral functions, except that it has been assumed that the imaginary part of the self-energy, although energy dependent, is independent of wave vector $\vec{k}$ and band index n.] The resulting distribution function, denoted by $\tilde{P}_0(E,\omega)$, can be written as a convolution over $P_0(E,\omega)$:

$$\tilde{P}_0(E,\omega) = \int dE'\, d\omega'\, P_0(E',\omega') A_e(E,E') \times A_h(E - \omega; E' - \omega') \quad \text{(C6)}$$

(the sharp edges at $E = E_f$ and $E = E_f + \omega$ are preserved if the spectral functions become δ functions at the Fermi energy). Including the lifetime broadening effects by convolution after the $\vec{k}$ integration is completed, rather than carrying out the $\vec{k}$ integration over the spectral functions, results in a substantial savings in computer time, and is an exact procedure as long as the imaginary part of the self-energy is independent of $\vec{k}$. This is probably an unrealistic assumption, but it is unlikely that any slight improvement in agreement with experiment resulting from the use of a $\vec{k}$-dependent relaxation time would justify the increased cost and complexity of the calculation. We have made tests of various procedures for including the spectral broadening, and have found that the distribution

$$\tilde{P}_0(E,\omega) = \int dE'\, P_0(E',\omega) A_h(E - \omega; E' - \omega) \quad \text{(C7)}$$

is usually indistinguishable from that given in Eq. (C6), and, since it involves no integration over ω, can be obtained at a still further substantial savings in computer time.

One can derive Eq. (C7) from Eq. (C6) by writing $P_0(E,\omega)$ as $P_1(E - \omega;\omega)$, and assuming the dependence on the first variable $(E - \omega)$ is strong, but neglecting the variation with the second variable (ω) over the widths of the electron and hole spectral functions. This assumption, which is appropriate to a material, such as a transition or noble metal, with a photoemission spectrum with a number of stationary peaks (over a range of ω of ~ 1 eV) in initial energy, leads to an expression [Eq. (C7)] which simply represents a broadening of the photoemission distributions on the energy variable. The only new feature incorporated here is that the width of the broadening function has the energy dependence implied by Kane's random-k model for

the hole lifetime. (A different way of saying this is that the calculations were found to be insensitive to broadening of the electron states, and it was found unnecessary to take this broadening into account.)

In practice, the photoemission distributions are calculated for each ω on a uniform mesh of energies E. Since convolution with a Lorentzian conserves area, it is important that the bare (infinite lifetime) photoemission distribution be calculated in such a way that it has the correct area. It was found that many of the fine-mesh cubes contribute only to rather narrow energy ranges, and it is thus possible to miss the contributions of such cubes altogether (if the contribution happens to fall between points on the energy mesh) or to grossly miscalculate their contributions to the area (if a mesh point happens to fall in the middle of a very sharp but very narrow peak). This situation is handled by finding the range of energy ΔE for which each band pair in each cube contributes to the photoemission; if ΔE is less than twice the spacing between points on the energy mesh, we compute the total area of the contribution (i.e., the integral over energy; this can be computed using the GR method) and add it into the photoemission distribution for the energy point nearest the center of gravity of the contribution.

After normalizing the distribution to one absorbed photon,

$$N_p(E,\omega)=\frac{\int dE' P_0(E',\omega)A_h(E-\omega;E'-\omega)}{\int dE' P_0(E',\omega)}\ , \tag{C8}$$

the next step is the calculation of the contribution of secondary electrons according to

$$N_s(E,\omega)=\int_E^{E_f+\omega} dE' S(E',E)N_p(E',\omega)\ . \tag{C9}$$

Here $S(E',E)$ is essentially the energy distribution function for secondary electrons at energy E produced by a primary electron at energy E' by electron-electron collisions.

In Kane's[32] random-k model, the matrix elements of the electron-electron interaction are taken to be constant, independent of $\vec{k}$ and band indexes. The $\vec{k}$-space integrals which occur in second-order perturbation theory can then all be contracted into densities of states. If we define

$$R(E)=\int_{E_f}^{E_f+E} dE' \rho_e(E')\rho_h(E'-E),\quad 0\le E \tag{C10}$$

$$T_e(E)=\int_{E_f}^{E} dE' \rho_e(E')R(E-E')\ ,\quad E\ge E_f \tag{C11}$$

$$T_h(E)=\int_{E}^{E_f} dE' \rho_h(E')R(E'-E)\ ,\quad E\le E_f \tag{C12}$$

where ρ_e and ρ_h are the densities of states for electrons and holes (simply the band densities of states above and below the Fermi energy), then Kane's result for the distribution function for secondary electrons is[32]

$$\tilde{S}(E',E)=2\rho_e(E)R(E'-E)/T_e(E')\ ,\quad E'\ge E>E_f \tag{C13}$$

the electron lifetime is

$$\tau_e(E)=\Lambda_e/T_e(E)\ , \tag{C14}$$

and the hole lifetime is

$$\tau_h(E)=\Lambda_h/T_h(E)\ , \tag{C15}$$

where Λ_e and Λ_h are constants. A desirable practical aspect of Kane's model is illustrated by Eq. (C13), where a matrix is given as a product of vectors, greatly reducing the storage requirement of the calculation.

Our calculations involve a number of further approximations. First, in a material with d bands, there is no reason to expect the electron-electron matrix elements between s states and d states to be similar; one would further expect matrix elements involving an odd number of d states to be smaller than those involving an even number of d states. In the noble metals, where the d states are completely below the Fermi energy, the pair-production process involves an odd number of d holes; since the matrix elements for such processes should be smaller than those involving only s states, one makes a large error by including the full d-band density of states in Eq. (C10). We have tacken this effect into account in an *ad hoc* fashion by cutting off the density of states in the d-band region at 6 states/Ry atom (or roughly twice the s-band density of states) in the calculations in Eqs. (C10)–(C12).

Second, the secondary distribution function used in Eq. (C9) is not that appearing in Eq. (C13), but is instead

$$\begin{aligned}S(E',E)&=[\tau_e(E)/\tau_e(E')]\tilde{S}(E',E)\\&=2\rho_e(E)R(E'-E)/T_e(E)\ .\end{aligned} \tag{C16}$$

The assumption is that, once a secondary electron has been produced, it moves without undergoing further pair-production processes (i.e., tertiaries, etc., are neglected). The transport factor for the secondary electrons should thus be evaluated at the energy E, rather than at the energy E' of the primaries. To the extent that αl in Eq. (C2) is small (which is true for transition and noble metals), multiplying by the ratio of relaxation times in Eq. (C16) takes this into account.

Third, if αl is small, $N_p(E,\omega)$ and $N_s(E,\omega)$ will both be proportional to Λ_e, the unknown constant in Eq. (C14) which fixes the size of the electron relaxation time. We can determine Λ_e, therefore,

by matching the energy integral of the theoretical photoemission distribution to the measured quantum yield at one photon frequency (we then use the same value of Λ_e for all other photon frequencies). The value of Λ_h in Eq. (C15), which fixes the size of the hole relaxation time, is chosen to give a reasonable match to the experimentally observed broadening of the photoemission distributions.

It is clear that much remains to be done in the theory of pair production; the distribution of secondaries calculated as discussed above is in only qualitative agreement with experiment. We have not tried to improve these calculations because our main interest is in the primary distributions, and because it appears that any substantial improvements in the treatment of the secondaries (for example, calculation of the electron-electron matrix elements) will require a major programing effort.

The final step in the calculations is the inclusion of surface-escape effects. Following Berglund and Spicer,[31] we put

$$\tilde{D}(E,\omega) = T_{\text{eff}}(E)[N_p(E,\omega) + N_s(E,\omega)] \tag{C17}$$

and use a free-electron model to find the surface-escape function $T_{\text{eff}}(E)$. That is,

$$T_{\text{eff}}(E) = \begin{cases} 0 & E \le E_f + \phi \\ \frac{1}{4}\left(1 - \frac{\phi}{E - E_f}\right), & E > E_f + \phi \end{cases} \tag{C18}$$

where ϕ is the work function. The distributions are then normalized by matching to the experimental quantum yield $Y(\omega_0)$ at one photon frequency ω_0, so that the final theoretical photoemission distributions are given by

$$D(E,\omega) = \frac{Y(\omega_0)\tilde{D}(E,\omega)}{\int dE\, \tilde{D}(E,\omega_0)} \ . \tag{C19}$$

As discussed above, this procedure fixes the value of the constant Λ_e appearing in the electron lifetime.

*Based in part on work sponsored by the U. S. Air Force Office of Scientific Research, Office of Aerospace Research, under Contract No. F44620-70-0089.

[1]M. I. Chodorow, Ph.D. thesis (MIT, 1939) (unpublished).
[2]J. C. Slater, Int. J. Quantum Chem. Symp. 5, 403 (1971), and references therein.
[3]J. F. Janak, A. R. Williams, and V. L. Moruzzi, Phys. Rev. B 6, 4367 (1972). A tabulation of this potential and charge density is available from the authors on request.
[4]L. J. Sham and W. Kohn, Phys. Rev. 145, 561 (1966).
[5]L. Hedin and B. I. Lundqvist, J. Phys. C 4, 2064 (1971).
[6]P. Hohenberg and W. Kohn, Phys. Rev. 136, B864 (1964).
[7]W. Kohn and L. J. Sham, Phys. Rev. 140, A1133 (1965).
[8]M. Rasolt and S. H. Vosko, Phys. Rev. Lett. 32, 297 (1974).
[9]K. Schwarz, Phys. Rev. B 5, 2466 (1972).
[10]K. S. Singwi, A. Sjölander, M. P. Tosi, and R. H. Land, Phys. Rev. B 1, 1044 (1970).
[11]J. C. Shaw, J. B. Ketterson, and L. R. Windmiller, Phys. Rev. B 5, 3894 (1972); O. K. Andersen, Phys. Rev. Lett. 27, 1211 (1971); D. Nowak and M. J. G. Lee, Phys. Rev. B 5, 2851 (1972).
[12]P. B. Johnson and R. W. Christy, Phys. Rev. B 6, 4370 (1972).
[13]F. M. Mueller and J. C. Phillips, Phys. Rev. 157, 600 (1967).
[14]A. R. Williams, J. F. Janak, and V. L. Moruzzi, Phys. Rev. Lett. 28, 671 (1972).
[15]P. O. Nilsson, Phys. Kondens. Mater. 11, 1 (1970).
[16]G. P. Pells and M. Shiga, J. Phys. C 2, 1835 (1969).
[17]U. Gerhardt, Phys. Rev. 172, 651 (1968).
[18]D. E. Eastman and J. K. Cashion, Phys. Rev. Lett. 24, 310 (1970).
[19]I. Lindau and L. Walldén, Solid State Commun. 9, 209 (1971); 9, 1147 (1971).
[20]D. E. Eastman and W. Grobman (private communication).
[21]V. L. Moruzzi, A. R. Williams, and J. F. Janak, Phys. Rev. B 8, 2546 (1973).
[22]A. R. Williams, J. F. Janak, and V. L. Moruzzi, J. Phys. (Paris) 33, C3-131 (1972).
[23]L. F. Wagner, W. E. Spicer, and S. Doniach, Solid State Commun. 15, 669 (1974).
[24]N. V. Smith and W. E. Spicer, Opt. Commun. 1, 157 (1969); N. V. Smith, Phys. Rev. Lett. 23, 1452 (1969).
[25]L. Hedin and S. Lundqvist, Solid State Phys. 23, 1 (1969).
[26]T. M. Rice, Ann. Phys. (N.Y.) 31, 100 (1965).
[27]L. Hedin, Phys. Rev. 139, A796 (1965).
[28]A. R. Williams, J. F. Janak, and V. L. Moruzzi, Phys. Rev. B 6, 4509 (1972).
[29]G. Gilat and L. J. Raubenheimer, Phys. Rev. 144, 390 (1966).
[30]J. F. Janak, D. E. Eastman, and A. R. Williams, in *Electronic Density of States*, Natl. Bur. Stand. Special Publication 323 (U.S. GPO, Washington, D.C., 1971), p. 181.
[31]C. N. Berglund and W. E. Spicer, Phys. Rev. 136, A1030 (1964); 136, A1044 (1964).
[32]E. O. Kane, Phys. Rev. 159, 624 (1967).